Technical Report

Dislocation Observation Technique Using SEM/ECCI Method

Takashige MORI* Takafumi AMINO
Shunsuke TANIGUCHI Takayuki YONEZAWA
Akira TANIYAMA

Abstract

Electron Channeling Contrast Imaging (ECCI), a type of backscattered electron imaging in scanning electron microscopy (SEM) that utilizes electron channeling effects arising from the relationship between the incident electron beam and crystal orientation, enables direct observation of lattice defects such as grain boundaries and dislocations in polished bulk specimens. In this study, dislocation structures in ferrite were observed using SEM/ECCI with precise control of the incident beam direction relative to the crystal planes. As a result, it was found that: (1) all dislocation contrasts observed in bright-field TEM images were also visible in SEM/ECCI; (2) dislocation contrast varied depending on the incident beam direction and accelerating voltage, indicating the existence of optimal imaging conditions; and (3) SEM/ECCI is applicable for characterizing dislocations and evaluating strain fields around dislocations, similar to TEM.

1. Introduction

Steel materials are widely used in structures and mechanical components that support social infrastructure, and therefore must exhibit a wide range of properties tailored to specific service environments and performance requirements. Among these, mechanical properties such as strength, toughness, ductility, and fatigue characteristics are critical criteria for material selection and design, as they directly govern material reliability and safety.

Dislocations are the primary carriers of plastic deformation that underlies these mechanical properties, and their behavior governs the mechanical response of materials. Consequently, the structure and dynamics of dislocations constitute critical analytical factors directly associated with improving the performance of steel materials.

In recent years, advances in high-precision techniques for observing and quantifying material microstructures have led to the diversification of dislocation analysis methods. Transmission electron microscopy (TEM) enables direct observation of atomic arrangements and dislocation lines at the nanoscale,[1] making it effective technique for analyzing local dislocation structures and quantitatively evaluating dislocation density. However, TEM requires thinning the sample to a thin film, involves advanced sample preparation techniques, and is limited by a restricted observable area. X-ray diffraction (XRD) enables non-destructive quantification of dislocation density and character in bulk materials,[2] and is therefore widely employed as a practical evaluation method in industrial applications. However, dislocation analysis using XRD has limited in spatial resolution and is unsuitable for a detailed understanding of local dislocation structures.

Against this background, numerous studies[3–6] have reported direct observations of lattice defects such as grain boundaries and dislocations, in polished bulk specimens using electron channeling contrast imaging (ECCI) in scanning electron microscopy (SEM). SEM-based electron channeling contrast imaging (SEM/ECCI) is a back-scattered electron (BSE) imaging technique in SEM that exploits electron channeling effects arising from the relationship between the incident electron beam and the crystal orientation.

To observe dislocation contrast in arbitrary regions using the SEM/ECCI method, the orientation relationship between the incident electron beam and the crystal must be precisely controlled so as to achieve channeling conditions under which the backscattered electron rocking curve reaches a local minimum.[7] However, few studies have systematically investigated the influence of the electron beam incidence direction on dislocation contrast in the SEM/ECCI method. Pang et al.[8] simulated the contrast of screw dislocations in tantalum as a function of the deviation parameter w. Kriaa et al.[9] reported that the apparent dislocation width varies with the incident electron beam direction within the Kikuchi band, even along the same reciprocal lattice vector **g**. Gutierrez[10] experimentally investi-

* Senior Researcher, Materials Characterization Research Lab., Advanced Technology Research Laboratories
1-8 Fuso-Cho, Amagasaki City, Hyogo Pref. 660-0891

gated the effect of w and concluded that channeling conditions with a large positive w value, such as $w > 1.5 \pm 0.5$, are optimal for observing dislocation contrast.

This paper presents the results[11] of a detailed investigation into changes in dislocation contrast in ferrite using SEM/ECCI, in which the electron beam incidence angle relative to the crystal plane was precisely controlled by employing a piezoelectric element as the driving unit.

2. Effect of the Angle of the Incident Electron Beam in the SEM/ECCI Method[11]

Figure 1 (a) shows ECC images acquired with varying the incident electron beam direction relative to the (200) crystal plane of the observed ferrite grains. Figure 1 (b) shows the BSE intensity as a function of the sample tilt angle α about the tilt axis parallel to the (200) plane at accelerating voltages of 15 and 30 kV. The BSE intensity represents the average over a 100 × 100 pixel area in the same region for each image (the red square region in Fig. 1 (a)). As the incident electron beam direction varied relative to the (200) plane, the BSE intensity exhibited pronounced changes in the vicinity of the Bragg condition. In this study, the tilt angle difference between the (200) and ($\bar{2}$00) Bragg positions in the ferrite was approximately 2.8° at 30 kV. In contrast, the tilt angle difference between the channeling positions was approximately 3.6°, corresponding to the incidence conditions where the BSE intensity reaches a local minimum. These experimental results in good agreement with calculated rocking curves of backscattered electron diffraction intensity near the Bragg condition,[7] indicating that the channeling condition is satisfied for deviation parameters $w > 0$, i.e., at incidence angles higher than the Bragg condition.

Dislocation observation using the SEM/ECCI method requires channeling conditions where the BSE intensity exhibits a local minimum. Accordingly, the dislocation contrast near the channeling conditions was investigated. **Figure 2** shows an ECC image obtained by varying the incident electron beam direction relative to the (10$\bar{1}$) crystal plane of the ferrite grain. The dislocation contrast was found to vary with the tilt angle α in the vicinity of the channeling conditions.

To quantitatively investigate the dislocation contrast near the channeling condition, the dislocation contrast intensity I_{dc} and width W_{dc} were evaluated. **Figure 3** shows an example of a BSE intensity profile for a dislocation indicated by the red arrow in Fig. 2. A line profile crossing the dislocation was obtained by averaging the BSE intensity over a 100 nm region of interest (ROI) defined along the dislocation line. The width of the ROI was adjusted for each dislocation.

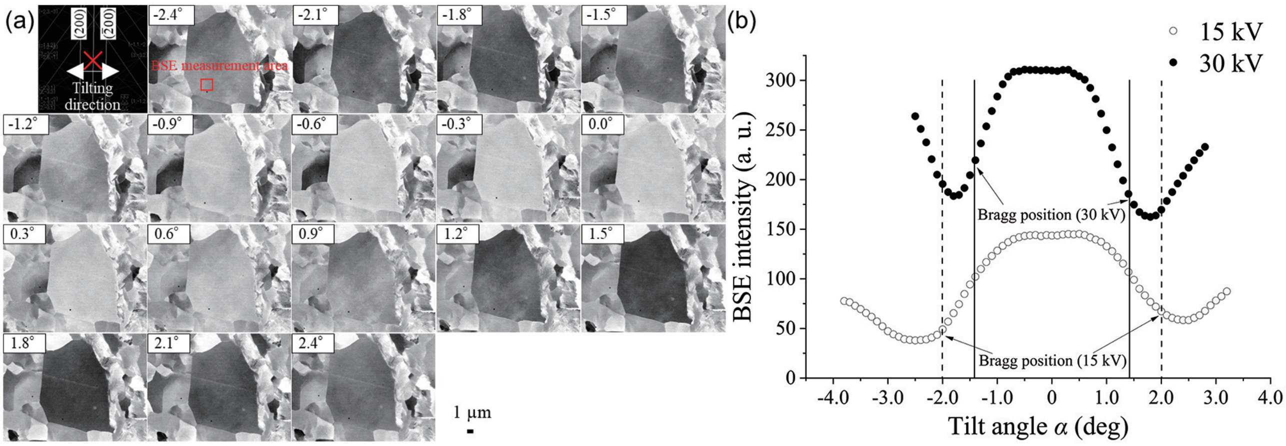

Fig. 1 BSE intensity as a function of the primary electron beam direction to the (200) crystal plane of a ferrite grain[11]

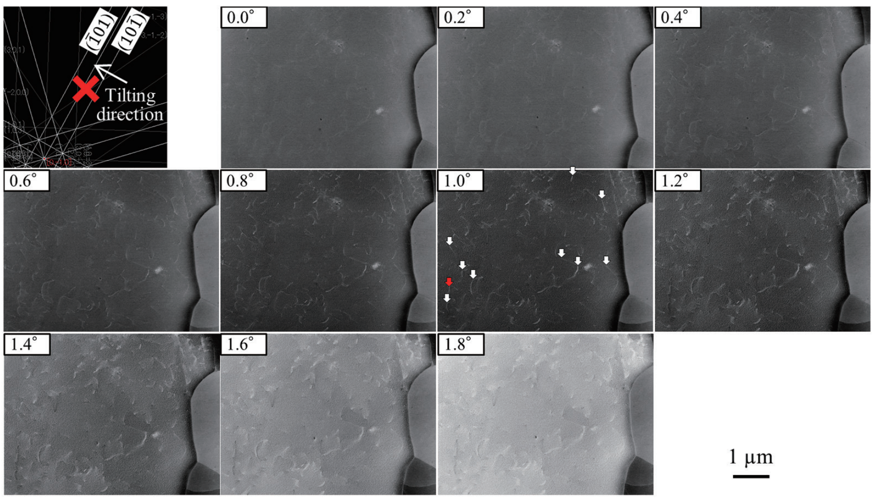

Fig. 2 Electron channeling contrast images obtained by changing the incident electron beam direction to the (10$\bar{1}$) crystal plane of ferrite grain at 30 kV[11]

I_{dc} was determined according to the following Equation (1).[10]

$$I_{dc} = (I_{max} - I_{min}) / (I_{max} + I_{min}) \quad (1)$$

where I_{max} and I_{min} are the maximum and minimum values of the BSE intensity profile crossing the dislocation, respectively. In this study, W_{dc} was evaluated as the full width at half maximum (FWHM) obtained by fitting a Gaussian function to the dislocation line profile.

For the ten dislocations indicated by the arrows in Fig. 2, I_{dc} and W_{dc} were evaluated from a series of ECC images acquired by varying the incident electron beam direction relative to the $(10\bar{1})$ crystal plane of the ferrite grains. Subsequently, the average values of these parameters for ECC images obtained at the same tilt angle were calculated and plotted as a function of the tilt angle α, together with the BSE intensity, as shown in **Fig. 4**.

For dislocation observation using the SEM/ECCI method, high I_{dc} and small W_{dc} are desirable. Both parameters exhibited clear dependence on the tilt angle α. While W_{dc} showed a valley-shaped minimum near the channeling condition, the maximum of I_{dc} was shifted away from the channeling condition, where the BSE intensity reaches a local minimum. These experimental results indicate that the strongest dislocation contrast is obtained at w values higher than those corresponding to the channeling condition. Under channeling conditions, the dislocation line width varied depending on the dislocation type, which is considered to reflect differences in the associated strain field arising from dislocation character, as described later.

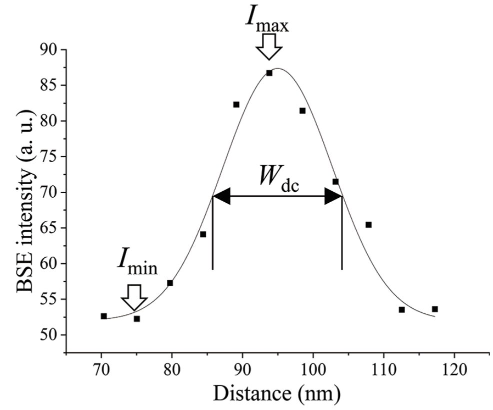

Fig. 3 Evaluation of dislocation contrast intensity I_{dc} and width W_{dc} [11]

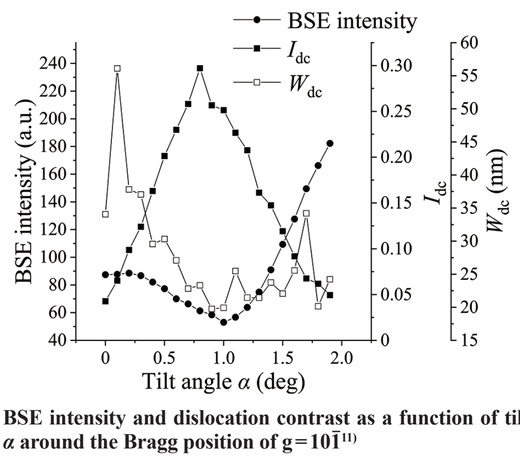

Fig. 4 BSE intensity and dislocation contrast as a function of tilt angle α around the Bragg position of $g = 10\bar{1}$ [11]

3. Effect of Accelerating Voltage on Dislocation Contrast in SEM/ECCI Method[11]

Research on the effect of acceleration voltage on dislocation contrast in the SEM/ECCI method is limited,[3, 12] and there is ongoing debate as to whether higher accelerating voltages have a positive or negative influence. Consequently, although dislocation observations using the SEM/ECCI method are performed at accelerating voltages of 10–30 kV, the optimal accelerating voltage condition has not been clearly defined.

As mentioned above, the tilt angle α required to satisfy the channeling condition varies with accelerating voltage. Therefore, when comparing the same field of view, repeated adjustment of the incident beam direction to meet the channeling condition is required. **Figure 5** shows ECC images of the same field of view acquired under strictly controlled channeling conditions at stepwise accelerating voltages ranging from 15 to 30 kV. For the 10 dislocations indicated by white arrows in the ECC images of Fig. 5, W_{dc} was evaluated using the method described above, and the average values with accelerating voltage are plotted in **Fig. 6**. Because the BSE intensity varies with accelerating voltage, brightness and contrast of the ECC images must be adjusted accordingly, rendering I_{dc} unsuitable for quantitative comparison.

At accelerating voltages of 15–25 kV, W_{dc} decreased with increasing accelerating voltage, whereas in the range of 25–30 kV, W_{dc} increased at 30 kV. As the accelerating voltage increases, the slope

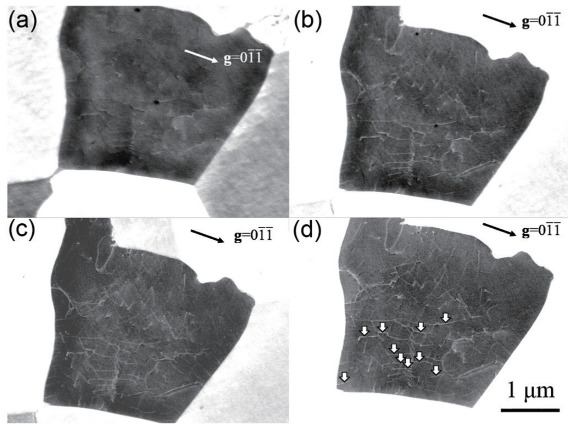

Fig. 5 ECC images of the same field of view obtained under stepwise accelerating voltages of (a) 15, (b) 20, (c) 25 and (d) 30 kV, strictly satisfying channeling conditions with $g = 0\bar{1}\bar{1}$ excitation

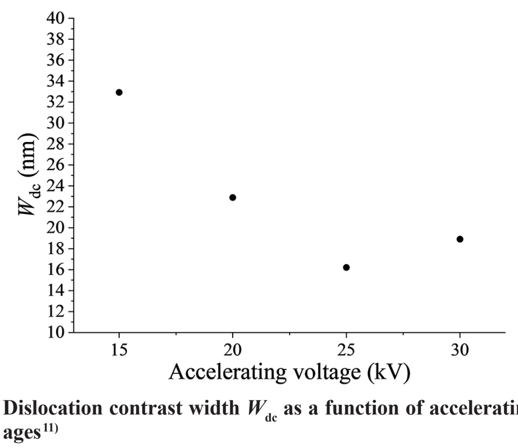

Fig. 6 Dislocation contrast width W_{dc} as a function of accelerating voltages[11]

of the BSE intensity near the Bragg position becomes steeper (Fig. 1). Therefore, the change in BSE intensity caused by local crystal rotation around the dislocation line under channeling conditions is considered to become more pronounced with increasing acceleration voltage up to 25 kV.

Furthermore, the electron beam probe size is also considered to be a factor influencing W_{dc}. In this study, all ECC images were acquired using the same working distance (WD) of 4 mm and an objective aperture diameter of 30 μm, ensuring an identical convergence angle of the electron probe. However, the convergence angle required to minimize the probe size depends on the accelerating voltage, mainly due to the influence of diffraction aberration and spherical aberration at higher acceleration voltages.[13] Therefore, the W_{dc} obtained at 30 kV is considered to be inferior to that at 25 kV. Since the convergence angle of the electron probe is affected by the objective aperture diameter, WD, and the electron optical system of the instrument, it is necessary to establish optimal observation conditions in addition to precise control of the incident electron beam direction.

4. Direct Comparison of Dislocation Contrast Between SEM/ECCI and Bright-Field TEM[11]

To verify the validity of the SEM/ECCI method for observing dislocation contrast, bright-field TEM (BF-TEM) observations were performed on the same thin foil containing ferrite grains. **Figure 7**(a) shows the BF-TEM image of a ferrite grain acquired from the front side of the thin foil under an excitation condition of **g** = 110. Figures 7(b)–(d) show ECC images of the ferrite grain acquired from the front and back sides of the thin foil under excitation with **g** = 110. In the BF-TEM image, each dislocation with endpoints was independently observed from the front and back sides of the thin foil. Here, the dislocations observed in the BF-TEM image were labeled i–x (Fig. 7(a)), and their correspondence with the dislocations in the ECC images (Fig. 7(b)–(d)) was confirmed. Particular attention was paid to the dislocations labeled viii and x. These dislocations were observed in the BF-TEM image (Fig. 7(a)) and in the ECC image acquired from the front side of the specimen (Fig. 7(b)), but were not observed in the ECC image acquired from the back side (Fig. 7(c)). This result indicates that the dislocations corresponding to viii and x are dislocations with endpoints at the surface and grain boundaries of the thin foil.

Furthermore, the dislocations labeled vii and ix were observed as continuous dislocation lines in the BF-TEM image (Fig. 7(a)). In contrast, no dislocation contrast was observed near the central regions of vii and ix in the ECC images. This is because these dislocations penetrate through the thin foil and intersect both the front and back surfaces. While the BF-TEM image acquired at 300 kV enables observation through the entire specimen thickness, the SEM/ECCI method operated at 30 kV has a shallow information depth, which prevents observation of extending throughout the full thickness of the specimen. The dislocation contrast obtained by BF-TEM and SEM/ECCI was acquired using the same diffraction vector and within the same field of view, showing good correspondence. These results experimentally demonstrate that the SEM/ECCI method, when strict channeling conditions are satisfied by precise control of the incident electron beam direction, enables the observation of individual dislocations in a manner comparable to that of the BF-TEM method.

5. Characterization of Dislocations by SEM/ECCI[11]

Figures 8(a)–(d) show ECC images acquired within the same field of view using three different reciprocal lattice vectors **g**. Figure 8(e) shows the inverse pole figure (IPF) map of the observed grains, whose orientation is close to $[11\bar{1}]$ relative to the specimen surface. The observed grain was slightly rotated about an axis parallel to $(1\bar{1}0)$ due to the presence of a small-angle grain boundary at its center. In Fig. 8(a), the upper region of the grain was imaged under channeling conditions. Subsequently, by tilting the specimen stage 0.8° about an axis parallel to $(1\bar{1}0)$, an ECC image of the lower region of the same grain was acquired (Fig. 8(b)). For example, in the ECC image obtained using the reciprocal lattice vector **g** = $\bar{1}0\bar{1}$, the dislocation contrast corresponding to the trace line of $[1\bar{1}\bar{1}]$ direction disappeared (Fig. 8, white arrow). Assuming that the Burgers vector **b** of dislocations in the ferrite grain corresponds to the closest-packed direction, **b** = $a/2\langle 111\rangle$ (where a is the lattice constant), the Burgers vectors **b** = $a/2 \pm [1\bar{1}\bar{1}]$ and **b** = $a/2[11\bar{1}]$ satisfy the invisibility condition $\mathbf{g}\cdot\mathbf{b} = 0$ for the reciprocal lattice vector **g** = $\bar{1}0\bar{1}$. Since the $\pm [11\bar{1}]$ direction is perpendicular to the surface of the observed grain, the Burgers vector **b** of the dislocation indicated by the white arrow can be identified as **b** = $a/2 \pm [1\bar{1}\bar{1}]$. Furthermore, because the dislocation line vector **u** is parallel to **b**, these dislocations are identified as screw dislocations with **b** = $a/2 \pm [1\bar{1}\bar{1}]$.

Similarly, characterization of the dislocations revealed that many of the dislocations exhibiting vanished contrast were screw dislocations. In Addition, edge dislocations, for which the Burgers vector **b** and the dislocation line vector **u** are mutually orthogonal, were also observed (Fig. 8, gray arrows).

Figure 9(a) shows a comparison of the dislocation contrast for dislocation s1 (screw dislocation) and e1 (edge dislocation) identified in Fig. 8. W_{dc} of the screw and edge dislocation indicated by the white and gray arrows in Fig. 8 were evaluated, and their respective average values are plotted in Fig. 9(b). A clear difference in W_{dc} was observed between the two dislocation types, with the contrast width of the edge dislocations exhibiting a wider contrast width than that of the screw dislocations.

According to BF-TEM image calculations based on dynamical

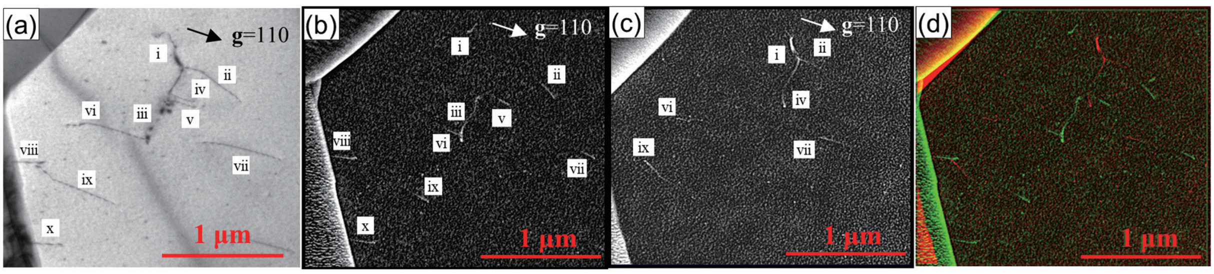

Fig. 7 Direct comparison of details in the dislocation contrast of bright-field (BF) TEM and ECC images[11]

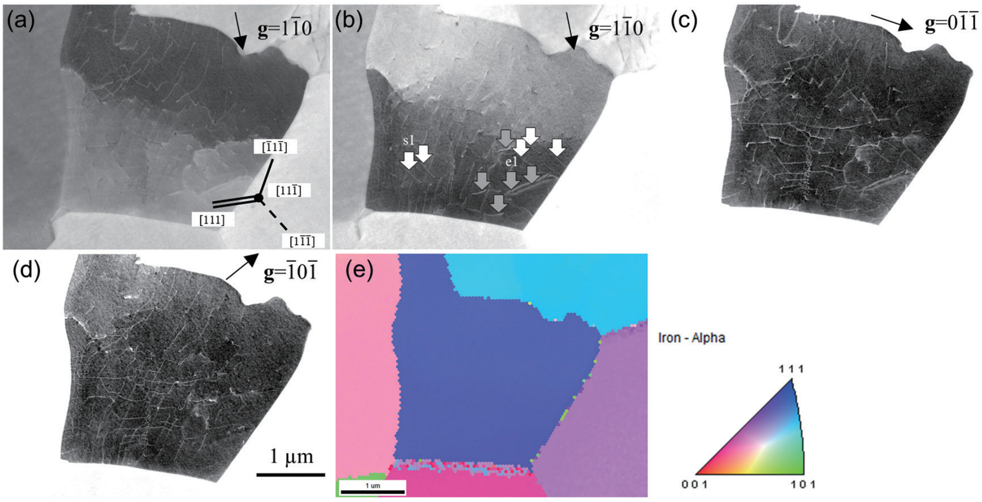

Fig. 8 Characteristic analysis of dislocations using the g·b = 0 invisibility criterion [11]

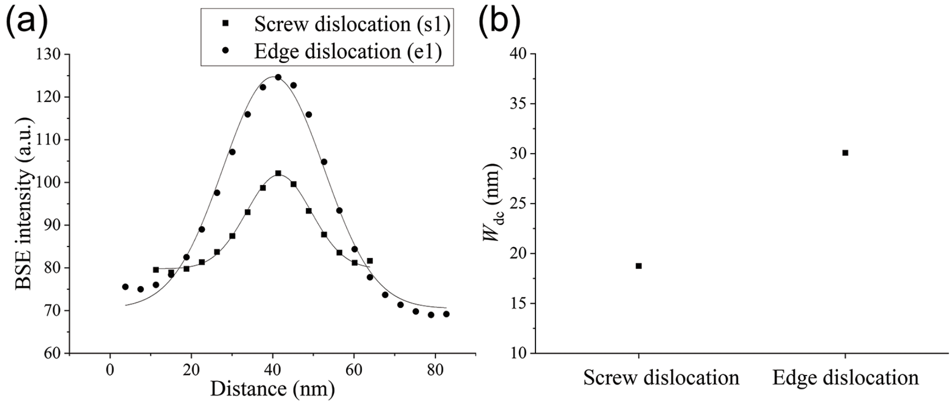

Fig. 9 Comparison of dislocation width of screw and edge dislocations [11]

diffraction theory,[14, 15] the width of a pure edge dislocation lying parallel to the specimen surface is approximately twice that of a pure screw dislocation. This difference originates from the distinct strain fields associated with each type of dislocation. The experimental results shown in Fig. 9 are consistent with the calculated BF-TEM images. Therefore, because the SEM/ECCI method enables precise control of the incident electron beam direction, it is an effective technique for dislocation characterization and for visualizing difference in strain fields between screw and edge dislocations, in a manner comparable to the TEM method.

6. Conclusion

This paper presented examples of detailed observation of dislocation structures in ferrite using the SEM/ECCI method. It demonstrated that all dislocation contrasts observed in bright-field TEM images can also be observed by SEM/ECCI; that dislocation contrast varies with the electron beam incidence angle relative to the crystal plane and with the accelerating voltage, and that optimal observation conditions exist; and that SEM/ECCI, similar to TEM, can be used for dislocation characterization and for evaluation the strain fields surrounding dislocations. By precisely controlling the direction of the incident electron beam relative to the crystal plane during SEM/ECCI observation, dislocation contrast comparable to that obtained by TEM can be achieved without the need for thin-foil specimen preparation. Furthermore, the applicability of the SEM/ECCI method is expected to expand, enabling more extensive observations, including dislocation contrast analysis in bulk specimens.

Acknowledgments

The authors gratefully acknowledge Professor Masaaki Sugiyama and Professor Naoki Maruyama of Osaka University for their valuable discussions and insightful guidance on data interpretation.

References

1) Taniguchi, S., Kameya, M., Kobayashi, Y., Ito, K., Yamasaki, S.: Tetsu-to- Hagané. 109, 438 (2023)
2) Yonemura. M., Inoue. K.: Metal. Mater. Trans. A 47, 6384 (2016)
3) Gutierrez-Urrutia, I., Zaefferer, S., Raabe, D.: Scri. Mater. 61, 737 (2009)
4) Mansour, H., Guyon, J., Crimp, M.A., Gey, N., Beausir, B., Maloufi, N.: Scri. Mater. 84-85, 11 (2014)
5) L'hôte, G., Lafond, C., Steyer, P., Deschanel, S., Douillard, T., Langlois, C., Cazottes, S.: Scri. Mater. 162, 103 (2019)
6) Takayama, A., Mori, T., Hayakawa, M., Nakayama, E., Kato, T., Makino, T., Maruyama, N., Yamamoto, M.: Journal of the Society of Materials Science, Japan. 73, 896 (2024)
7) Zaefferer, S., Elhami, -N-N.: Acta Mater. 75, 20 (2014)
8) Pang, B., Jones, P., Chiu, Y., Millett, J.C.F., Whiteman, G.: Philos. Mag. 97 346 (2017)
9) Kriaa, H., Guitton, A., Maloufi, N.: Sci. Rep. 7, 9742 (2017)
10) Gutierrez-Urrutia, I.: Ultramicroscopy. 206, 112826 (2019)
11) Mori, T., Amino, T., Yokoyama, C., Taniguchi, S., Yonezawa, T., Taniya-

ma, A.: Microscopy. 73, 308 (2023)
12) Kamaladasa, R.J., Liu, F., Porter, L.M., Davis, R.F., Koleske, D., Mulholland, G., Jones, K.A., Picard, Y.N.: J. Microsc. 244, 311 (2011)
13) Reimer, L.: Scan Electron Microscopy. Springer, Berlin, 1985
14) Howie, A., Whelan, M.J.: Proc. Roy. Soc. A 267, 206 (1962)
15) Hirsch, P.B., Howie, A., Nicholson, R., Pashley, D.W., Whelan, M.J.: Electron Microscopy of Thin Crystals. Butterworths, Boston, 1965

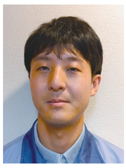

Takashige MORI
Senior Researcher
Materials Characterization Research Lab.
Advanced Technology Research Laboratories
1-8 Fuso-Cho, Amagasaki City, Hyogo Pref. 660-0891

Takafumi AMINO
Dr. Eng., General Manager, Head of Section
Materials Characterization Research Lab.
Advanced Technology Research Laboratories

Shunsuke TANIGUCHI
Senior Researcher
Materials Characterization Research Lab.
Advanced Technology Research Laboratories

Takayuki YONEZAWA
Ph.D. in Engineering, Senior Manager
Plate Technology Div.
Plate & Construction Products Unit

Akira TANIYAMA
Ph.D, Executive Director, Secretary-General
The Japan Institute of Metals and Materials
(Former General Manager, Head of Dept.
Materials Characterization Research Lab.
Advanced Technology Research Laboratories)